

Personalized Federated Learning for Spatio-Temporal Forecasting: A Dual Semantic Alignment-Based Contrastive Approach

Qingxiang Liu¹ Sheng Sun¹ Yuxuan Liang² Jingjing Xue¹ Min Liu¹

Abstract

The existing federated learning (FL) methods for spatio-temporal forecasting fail to capture the inherent spatio-temporal heterogeneity, which calls for personalized FL (PFL) methods to model the spatio-temporally variant patterns. While contrastive learning approach is promising in addressing spatio-temporal heterogeneity, the existing methods are noneffective in determining negative pairs and can hardly apply to PFL paradigm. To tackle this limitation, we propose a novel PFL method, named **F**ederated **d**Ual **s**Emantic **a**Lignment-based **c**ontra**S**tive learning (FUELS), which can adaptively align positive and negative pairs based on semantic similarity, thereby injecting precise spatio-temporal heterogeneity into the latent representation space by auxiliary contrastive tasks. From temporal perspective, a hard negative filtering module is introduced to dynamically align heterogeneous temporal representations for the supplemented intra-client contrastive task. From spatial perspective, we design lightweight-but-efficient prototypes as client-level semantic representations, based on which the server evaluates spatial similarity and yields client-customized global prototypes for the supplemented inter-client contrastive task. Extensive experiments demonstrate that FUELS outperforms state-of-the-art methods, with communication cost decreasing by around 94%.

1. Introduction

Spatio-temporal forecasting aims at predicting the future trends with historical records from distributed facilities. Actually, the facilities may be deployed by different organiza-

¹Institute of Computing Technology, Chinese Academy of Sciences, Beijing, China ²The Hong Kong University of Science and Technology (Guangzhou). Correspondence to: Min Liu <liumin@ict.ac.cn>.

Preliminary work.

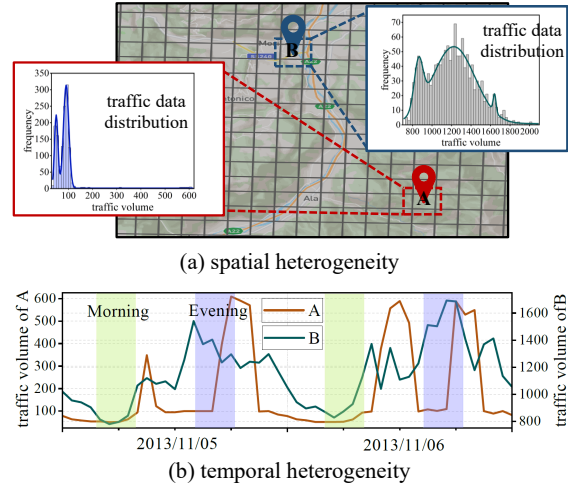


Figure 1. Spatio-temporal heterogeneity inside traffic flows.

tions and therefore the collected data can hardly be uploaded to a public server for training due to copyright protection. For example, in wireless traffic prediction, different telecom operators may hesitate to share access to traffic data of base stations (BSs) to others. Federated Learning (FL) enables clients to collaboratively optimize a shared model without the disclosure of private data and simultaneously can achieve comparable performance with centralized learning methods (McMahan et al., 2017). Therefore, FL generates great promise in the task of spatio-temporal forecasting and many sophisticated FL methods have been proposed to effectively evaluate the spatio-temporal correlation (Li et al., 2021c; Li & Wang, 2022). Given that the server has only access to local model parameters, these FL methods cannot exploit a joint spatio-temporal correlation-capturing module like centralized methods (Li et al., 2018; Li & Zhu, 2021). In general, most of them decouple the spatio-temporal correlation, and evaluate spatial correlation in the server by Graph Neural Networks (Zhao et al., 2020; Lin et al., 2021) and temporal correlation at local clients by Recurrent Neural Networks (Zhu & Wang, 2021; Mahdy et al., 2020).

Nevertheless, these FL forecasting methods cannot capture the inherent spatio-temporal heterogeneity by adopting

shared model parameters across clients. As shown in Figure 1, traffic patterns are spatio-variant (*traffic distribution of two clients varies*) and time-variant (*traffic patterns in the morning and evening are diverse*). The spatio-temporal heterogeneous traffic patterns call for personalized federated learning (PFL) methods to tackle with differentiated representations in the latent space from spatio-temporal level. However, current PFL methods all focus on increasing the generalization ability of local models by sharing diverse knowledge across clients (Karimireddy et al., 2020; Tan et al., 2022a; Chen et al., 2023), which can hardly work on coupled spatio-temporal heterogeneity.

Contrastive learning has emerged as an effective technique which shows great promise in improving PFL paradigm to address spatio-temporal heterogeneity. Generally, contrastive learning can maximize the agreement between similar semantic representations (*positive pairs*), which can increase representations’ differentiation, thereby injecting spatio-temporal heterogeneity into the latent representation space. Since there are no explicit semantic labels in spatio-temporal forecasting like the task of image classification, it is a challenge to determine positive and negative pairs. In (Ji et al., 2023), for spatial heterogeneity, learnable embeddings are introduced for clustering regions’ representations, which can hardly apply to PFL paradigm, due to the exposure of raw data and frequent communication in the process of parameter optimization. For temporal heterogeneity, region-level and city-level representations of the same time stamps make up positive pairs, otherwise negative pairs, which ignores semantic similarity among representations of different time stamps (termed *hard negatives*). Therefore, **it remains a question how to exactly determine negative and positive pairs when adopting contrastive learning in PFL paradigm for tackling spatio-temporal heterogeneity.**

To this end, we propose a novel PFL method, named **F**ederated **d**ual **s**emantic **a**lignment-based **c**ontrastive learning (FUELS), which can dynamically establish positive and negative pairs based on spatio-temporal representations’ similarity, hence guaranteeing the validity of spatio-temporal heterogeneity modeling. From temporal perspective, we propose a hard negative filtering module for each client, which can adaptively align true negative pairs for intra-client contrastive task so as to inject temporal heterogeneity into temporal representations. From spatial perspective, we define prototypes as client-level semantic representations and directly serve as the communication carrier, which enables sharing denoising knowledge across clients in a communication-efficient manner. We propose a Jensen Shannon Divergence (JSD)-based aggregation mechanism, which firstly aligns homogeneous and heterogeneous prototypes from clients and then yields client-customized global positive and negative prototypes for inter-client contrastive task to increase the spatial differentiation of local

models.

We summarize the key contributions as follows.

- To the best of our knowledge, this is the first PFL method towards spatio-temporal heterogeneity, where local training is enhanced by two well-crafted contrastive loss items to increase prediction models’ ability of discerning spatial and temporal heterogeneity.
- We design a hard negative filtering module to dynamically evaluate the heterogeneous degree among temporal representations and establish true negative pairs.
- We propose a JSD-based aggregation mechanism to generate particular global positive and negative prototypes for clients, striking a balance between sharing semantic knowledge and evaluating spatial heterogeneity.
- We validate the effectiveness and efficiency of the proposed FUELS from both theoretical analysis and extensive experiments. The numerical results show that FUELS can achieve consistently superior forecasting performance and simultaneously decrease the communication cost by around 94%.

2. Problem Formulation

One typical task of spatio-temporal forecasting is wireless traffic prediction. Given N BSs as clients in the FL paradigm, the n -th BS has its traffic observations $\mathcal{V}_n = \{v_n^k | k \in [1, K]\}$, where $v_n^k \in \mathbb{R}$ denotes the detected traffic volume of client n at the k -th time stamp. Based on sliding window mechanism (Zhang et al., 2021), \mathcal{V}_n can be divided into input-output pairs (samples), which is denoted as $\mathcal{D}_n = \{(\mathbf{x}_n^k; y_n^k)\}$. Thereinto, $y_n^k = v_n^k$ denotes the value to be predicted. $\mathbf{x}_n^k = (\mathbf{c}\mathbf{v}_n^k; \mathbf{p}\mathbf{v}_n^k)$, where $\mathbf{c}\mathbf{v}_n^k \in \mathbb{R}^c$, $\mathbf{p}\mathbf{v}_n^k \in \mathbb{R}^q$, and $\mathbf{x}_n^k \in \mathbb{R}^{c+q}$. $\mathbf{c}\mathbf{v}_n^k = (v_n^{k-c}, \dots, v_n^{k-2}, v_n^{k-1})$ and $\mathbf{p}\mathbf{v}_n^k = (v_n^{k-qp}, \dots, v_n^{k-2p}, v_n^{k-p})$ denote two historical traffic sequences to evaluate the closeness and periodicity of traffic data. c , q , and p represent the size of close window, the size of periodic window, and the periodicity of traffic volume.

Since BSs are deployed at different locations, such as downtown area and suburb *etc.*, the detected traffic data across different BSs have diverse distributions. Therefore, in PFL paradigm, each BS tends to learn its own prediction model for performance improvement. The objective can be formulated as

$$\min_{\{w_n\}} \frac{1}{N} \sum_{n=1}^N \frac{|\mathcal{D}_n|}{D} \sum_{(\mathbf{x}_n^k, y_n^k) \in \mathcal{D}_n} \mathcal{L}(f(w_n; \mathbf{x}_n^k), y_n^k). \quad (1)$$

where $f(\cdot)$ represents prediction model. $\mathcal{L}(\cdot)$ denotes the loss function. $D = \sum_{n=1}^N |\mathcal{D}_n|$ denotes the total number of

samples over all N clients. $w_n(1 \leq n \leq N)$ denotes the model parameters of client n .

3. Methodology

We firstly provide an overarching depiction of FUELS, as shown in Figure 2. In macroscopic view, local training is enhanced by two designed contrastive loss items (Figure 2 (a)). From temporal perspective, we propose a hard negative filtering module for true negative alignment. From spatial perspective, we employ prototypes as communication carrier (Figure 2 (b)), and generate specific global prototypes (Figure 2 (c)) for spatial heterogeneity evaluation. We elaborate the technical details in the following parts.

3.1. Encoder and Decoder

In FUELS, we split the prediction model f into two components. (i) *encoder* $en(\delta_n; \mathbf{x}_n) : \mathbb{R}^{B \times (c+q)} \rightarrow \mathbb{R}^{B \times d_r}$, is parameterized by δ_n and maps \mathbf{x}_n into a latent space with d_r dimensions, where $(\mathbf{x}_n, \mathbf{y}_n)$ denotes a batch of training samples from \mathcal{D}_n with batch size B . Actually, $\mathbf{x}_n = (\mathbf{c}\mathbf{v}_n, \mathbf{p}\mathbf{v}_n)$, where $\mathbf{c}\mathbf{v}_n \in \mathbb{R}^{B \times c}$ and $\mathbf{p}\mathbf{v}_n \in \mathbb{R}^{B \times p}$. we adopt two widely used Gated Recurrent Unit (GRU) models to evaluate the closeness and periodicity from $\mathbf{c}\mathbf{v}_n$ and $\mathbf{p}\mathbf{v}_n$, denoted as closeness-GRU (GRU_c) and periodicity-GRU (GRU_p) respectively. GRU_c($\delta_n^c; \mathbf{c}\mathbf{v}_n$): $\mathbb{R}^{B \times c} \rightarrow \mathbb{R}^{B \times \frac{d_r}{2}}$, is parameterized by δ_n^c . GRU_p($\delta_n^p; \mathbf{p}\mathbf{v}_n$): $\mathbb{R}^{B \times p} \rightarrow \mathbb{R}^{B \times \frac{d_r}{2}}$, is parameterized by δ_n^p . We denote the **representation** of \mathbf{x}_n output by the encoder en as $r_n \in \mathbb{R}^{B \times d_r}$, which can be formulated as

$$\begin{aligned} r_n &= en(\delta_n; \mathbf{x}_n) \\ &= \text{concat} [\text{GRU}_c(\delta_n^c; \mathbf{c}\mathbf{v}_n); \text{GRU}_p(\delta_n^p; \mathbf{p}\mathbf{v}_n)]. \end{aligned} \quad (2)$$

(ii) *decoder* $de(\phi_n; \cdot) : \mathbb{R}^{B \times d_r} \rightarrow \mathbb{R}^B$, is parameterized by ϕ_n and generates the final predicted result $\hat{\mathbf{y}}_n$ from the representation, i.e., $\hat{\mathbf{y}}_n = de(\phi_n; r_n)$. Similar with many prediction methods, we adopt the fully connected layers as the decoder de .

3.2. Intra-Client Contrastive Task for Temporal Heterogeneity

In (Liu et al., 2022), hard negatives are filtered out based on traffic closeness but those out of the preset closeness scope are still utilized to form negative pairs and may perturb the latent semantic space. Therefore, we propose a hard negative filtering module to align representations by semantic similarity and then design an intra-client contrastive task to maximize the divergence of negative pairs, thereby injecting precise temporal heterogeneity into temporal representations.

Firstly, we adopt the temporal shifting manner in (Liu et al.,

2022) to generate the augmented dataset for client n , which is denoted as \mathcal{D}'_n . For \mathbf{x}_n , the corresponding augmented batch in \mathcal{D}'_n is denoted as \mathbf{x}'_n . The representation of \mathbf{x}'_n is denoted as $r'_n \in \mathbb{R}^{B \times d_r}$. Let $r'_{n,i} \in \mathbb{R}^{d_r}$ denote the i -th row of r'_n , i.e., the temporal representation of the i -th time stamp of \mathbf{x}'_n .

The procedure of hard negative filtering is formulated as

$$SM = \exp(\text{sim}(r_n, r'_n) / \tau), \quad (3)$$

$$Z = \text{ReLU}(SM \odot W_n), \quad (4)$$

$$\mathcal{TN}_b = \{i | Z_{b,i} > 0\}, \quad (5)$$

where $SM \in \mathbb{R}^{B \times B}$ denotes the similarity matrix, $\text{sim}(\cdot, \cdot)$ denotes the cosine similarity and τ denotes the temperature factor. $W_n \in \mathbb{R}^{B \times B}$ denotes the learnable filtering matrix and \odot denotes the Hadamard product. If $Z_{b,i} = 0 (i \neq b)$, we treat $r'_{n,i}$ as a hard negative of $r_{n,b}$. If $Z_{b,i} > 0$, $r'_{n,i}$ is seen as a true negative of $r_{n,b}$ and i is added into \mathcal{TN}_b . Ideally, $Z_{b,b} (1 \leq b \leq B)$ should be equal to 0 as we also filter out the positive pairs by W_n (detailed results in Section 5.5).

By this procedure, representations of different time stamps but similar semantics can also be filtered out. The subsequent contrastive task will repel the representations with diverse semantics so as to validly inject temporal heterogeneity into representations. Finally, we can obtain the intra-client contrastive loss item as

$$\mathcal{L}_{intra} = \frac{1}{B} \sum_{b=1}^B -\log \frac{SM_{b,b}}{SM_{b,b} + \sum_{i \in \mathcal{TN}_b} Z_{b,i}}, \quad (6)$$

where $SM_{b,b}$ represents the similarity of positive pair and $Z_{b,i}$ denotes that of negative pair. Under the constraint of \mathcal{L}_{intra} , the prediction model will generate traffic representations with great temporal distinguishability.

3.3. Inter-Client Contrastive Task for Spatial Heterogeneity

In this section, we focus on how to preserve the spatial heterogeneity in the communication carrier of FL paradigm and fulfill the aim of assisting local optimization and simultaneously modeling spatial heterogeneity by shared knowledge across clients.

3.3.1. LOCAL PROTOTYPE DEFINITION

In conventional FL paradigm, model parameters serve as communication carrier, which are not compact and hardly preserve the spatial heterogeneity. Inspired by prototype learning, where prototypes represent the representations of samples with the same labels and thus can carry the class-specific semantic knowledge, we can extract the client-level prototype to carry the client-specific knowledge.

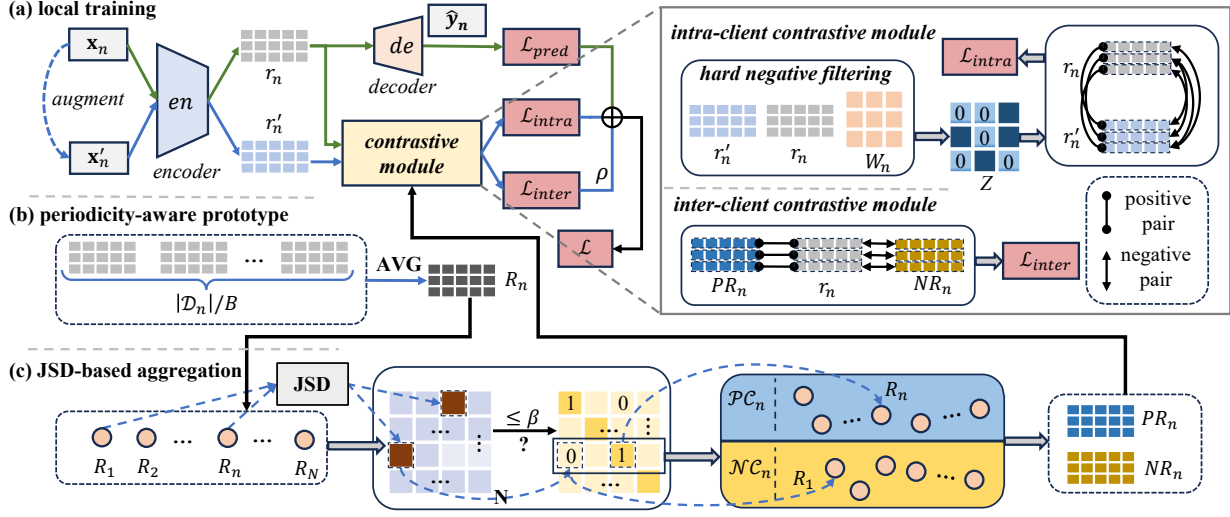


Figure 2. An overview of the proposed FUELS. (a) Each client performs local training by the supplemented inter- and intra-client contrastive loss items for spatio-temporal heterogeneity. (b) The designed periodicity-aware prototype works as the communication carrier. (c) The JSD-based aggregation generates client-customized global prototypes.

To achieve this goal, we start with a concatenation-based prototype, which is formulated as

$$R_n = \text{concat} [r_n | r_n = \text{en}(\mathbf{x}_n), \forall (\mathbf{x}_n, \mathbf{y}_n) \in \mathcal{D}_n], \quad (7)$$

where R_n denote the local prototype of client n . \mathcal{D}_n can be divided into $|\mathcal{D}_n|/B$ batches, with batch size equal to B and hence $R_n \in \mathbb{R}^{|\mathcal{D}_n| \times d_r}$. Each client should transmit $|\mathcal{D}_n| \times d_r$ parameters to the server at each training round, which potentially incurs more communication overhead than conventional FL methods with \mathcal{D}_n increasing.

Given the periodicity of traffic data, if we set the batch size B equal to the traffic periodicity p , representations of different batches will have similar distribution, as they all carry the traffic knowledge within a periodicity. Therefore, we can fuse these representations from different batches to obtain the periodicity-aware prototype as

$$R_n = \text{AVG} [r_n | r_n = \text{en}(\mathbf{x}_n), \forall (\mathbf{x}_n, \mathbf{y}_n) \in \mathcal{D}_n], \quad (8)$$

where **AVG** represents the averaging operation. Therefore, $R_n \in \mathbb{R}^{B \times d_r}$. The number of communication parameters keeps stable regardless of local dataset size, and is significantly fewer than the parameter size of local prediction model (see Section 5.2). Furthermore, compared with the aforementioned concatenation-based prototype, the periodicity-aware prototype is less affected by traffic noise and thus contains more available client-specific knowledge. *Therefore, in FUELS, we adopt the periodicity-aware prototype as communication carrier, unless otherwise stated.*

3.3.2. JSD-BASED AGGREGATION

For each client, the aggregation process in FUELS can align the homogeneous and heterogeneous semantic prototypes so

as to help model the spatial homogeneity and heterogeneity with others in the auxiliary contrastive task.

The diversity of traffic data across clients results in the distribution difference over $R_n (1 \leq n \leq N)$, which can be evaluated by JSD at the server. Let $JS(R_n || R_m) \in \mathbb{R}$ denote the JSD value between R_n and R_m . According to the calculation logic, if the heterogeneity between R_n and R_m is stronger, $JS(R_n || R_m)$ will be higher. Given a threshold β , if $JS(R_n || R_m) \leq \beta$, the server considers client n and m share similar knowledge and have homogeneous traffic data. Then, R_m will be added into \mathcal{PC}_n , which denotes the set of positive prototypes for client n . Otherwise, R_m will be put into \mathcal{NC}_n , which denotes the set of negative prototypes for client n . Finally, the server performs customized aggregation for client n as

$$PR_n = \frac{1}{|\mathcal{PC}_n|} \sum_{R_m \in \mathcal{PC}_n} R_m, \quad (9)$$

$$NR_n = \frac{1}{|\mathcal{NC}_n|} \sum_{R_m \in \mathcal{NC}_n} R_m, \quad (10)$$

where $PR_n \in \mathbb{R}^{B \times d_r}$ and $NR_n \in \mathbb{R}^{B \times d_r}$ represent the global positive and negative prototypes for client n .

It is worth noting that the computation complexity of JSD values is $\mathcal{O}\left(\frac{N^2 - N}{2}\right)$, which can hardly apply to forecasting tasks with masses of clients. The server can randomly select several clients as participants each round, with the selection ratio is α . Therefore, the JSD values of those clients which are not selected can be reused. The computation complexity can be reduced by $\mathcal{O}\left(\frac{N^2(1-\alpha)^2 - N(1-\alpha)}{2}\right)$. The reduction

enlarges significantly with N increasing.

3.3.3. INTER-CLIENT CONTRASTIVE LOSS

After aggregation, the customized global positive and negative prototypes are distributed to the corresponding clients. Each client can further enforce the spatial discrimination of its local prediction model by approaching the positive prototype and keeping away from the negative prototype in the training process.

We define the inter-client contrastive loss item as

$$\mathcal{L}_{inter} = \frac{1}{B} \sum_{b=1}^B -\log \frac{loss_{pos}}{loss_{pos} + loss_{neg}}, \quad (11)$$

$$loss_{pos} = \exp(\text{sim}(r_{n,b}, PR_{n,b}) / \tau), \quad (12)$$

$$loss_{neg} = \exp(\text{sim}(r_{n,b}, NR_{n,b}) / \tau), \quad (13)$$

where $PR_{n,b} \in \mathbb{R}^{d_r}$ and $NR_{n,b} \in \mathbb{R}^{d_r}$ denote the b -th row of PR_n and NR_n respectively. Under the constraint of \mathcal{L}_{inter} , the prediction model of the n -th client can be empowered with great spatial personalization.

3.4. Local Training and Inference

In the training process, client n inputs the representation r_n from the encoder en to the decoder de for generating the predicted values. Then, it calculates the prediction loss as

$$\mathcal{L}_{pred}(\delta_n; \phi_n; \mathbf{y}_n, \hat{\mathbf{y}}_n) = \frac{1}{B} \|\mathbf{y}_n - \hat{\mathbf{y}}_n\|^2. \quad (14)$$

Therefore, the local loss function \mathcal{L} in Eq. (1) is defined as a combination of \mathcal{L}_{intra} , \mathcal{L}_{inter} , and \mathcal{L}_{pred} , which is formulated as

$$\begin{aligned} \mathcal{L}(\delta_n, \phi_n, W_n; \mathbf{x}_n, \mathbf{y}_n, \mathbf{x}'_n, PR_n, NR_n) \\ = \mathcal{L}_{pred}(\delta_n, \phi_n; \mathbf{x}_n, \hat{\mathbf{y}}_n) \\ + \mathcal{L}_{intra}(\delta_n, W_n; \mathbf{x}_n, \mathbf{x}'_n) \\ + \rho \mathcal{L}_{inter}(\delta_n; \mathbf{x}_n, PR_n, NR_n), \end{aligned} \quad (15)$$

where ρ denotes the additive weight of \mathcal{L}_{inter} . Then, client n performs gradient descent to update local parameters. The training process of FUELS is elaborated in Appendix B. After the training process, the local encoders are of great personalization to generate spatio-temporal heterogeneous representations. Therefore, in the inference process, each client just needs to input the representations into the decoder to obtain the prediction results.

4. Algorithm Analysis

4.1. Generalization Analysis

We provide insights into the generalization bound of FUELS. The detailed proof and derivations are presented in

Appendix C.1. For ease of notation, we use the shorthand $\mathcal{L}(w_n) := \mathcal{L}(\delta_n, \phi_n, W_n; \mathbf{x}_n, \mathbf{y}_n, \mathbf{x}'_n, PR_n, NR_n)$.

Assumption 4.1. (*Bounded Maximum*) The Loss function $\mathcal{L}(\cdot)$ has an upper bound, i.e., $\max \mathcal{L}(\cdot) \leq C, C < \infty$.

Theorem 4.2. (*Generalization Bounded*) Let $w_n^*, n \in [1, N]$ denote the optimal model parameters for client n by FUELS. Denote the prediction model f as a hypothesis from \mathcal{F} and d as the VC-dimension of \mathcal{F} . With the probability at least $1 - \kappa$:

$$\begin{aligned} \max_{(w_1, \dots, w_N)} \left[\sum_{n=1}^N \frac{|\mathcal{D}_n|}{D} \mathcal{L}(w_n) - \sum_{n=1}^N \frac{|\mathcal{D}_n|}{D} \mathcal{L}(w_n^*) \right] \\ \leq \sqrt{\frac{2d}{D}} \log \frac{eD}{d} + \sqrt{\frac{C^2 D^2}{2}} \log \frac{1}{\kappa}, \end{aligned} \quad (16)$$

where e denotes the Euler's number. Theorem 4.2 indicates that the performance gap between FUELS and the optimal parameters is related to the VC-dimension of \mathcal{F} , which can be narrowed by carefully-selected prediction networks.

4.2. Convergence Analysis

Assumption 4.3. (*Bounded Expectation of Gradients*) The expectation of gradient of loss function $\mathcal{L}(\cdot)$ is uniformly bounded, i.e., $\mathbb{E}(\|\nabla \mathcal{L}(\cdot)\|) \leq G$.

Assumption 4.4. (*Lipschitz Smooth*) The loss function \mathcal{L} is L_1 -smooth, i.e., $\mathcal{L}(w) - \mathcal{L}(w') \leq \langle \nabla \mathcal{L}(w'), w - w' \rangle + L_1 \|w - w'\|^2, \forall w, w', \exists L_1 > 0$.

Assumption 4.5. (*Lipschitz Continuity*) Suppose $h : \mathcal{A}_1 \times \mathcal{A}_2 \times \dots \rightarrow \mathcal{A}_T$ is Lipschitz Continuous in \mathcal{A}_j , i.e., $\exists L_h, \forall a_j, \hat{a}_j \in \mathcal{A}_j, \|h(a_1, \dots, a_j, \dots) - h(a_1, \dots, \hat{a}_j, \dots)\| \leq L_h \|a_j - \hat{a}_j\|$.

Let $w_{n,t}^i$ denote the local model parameters of client n at the i -th iteration in the t -th FL round, where $0 \leq t \leq T - 1$ and $0 \leq i \leq I - 1$. T and I denote the total number of FL rounds and local iterations respectively.

Theorem 4.6. (*Convergence Rate*) Let Assumption 4.3 to 4.5 hold. Let $\mathcal{L}(w_{n,0}^0) - \mathcal{L}(w_n^*) = \Lambda$. If clients adopt stochastic gradient descent method to optimize local prediction models with the learning rate equal to η , for any client, given $\xi > 0$, after

$$T = \frac{\Lambda}{\xi I (\eta - L_1 \eta^2) - \rho \eta L_h N \alpha I^2 G} \quad (17)$$

FL rounds, we can obtain

$$\frac{1}{TI} \sum_{t=0}^{T-1} \sum_{i=0}^{I-1} \mathbb{E} \left[\|\nabla \mathcal{L}(w_{n,t}^i)\|^2 \right] < \xi \quad (18)$$

with

$$\eta < \frac{\xi - \rho L_h N \alpha I G}{L_1 \xi}. \quad (19)$$

Based on the above commonly-used assumptions in FL works (Kairouz et al., 2021), Theorem 4.6 (the detailed proof is presented in Appendix C.2) provides the convergence rate of FUELS. By adopting the learning rate η computed via Eq. (19), after T FL rounds (calculating T via Eq. (17)), the expectation of model updates will not exceed the given arbitrary value ξ .

4.3. Communication and Computation Complexity

The number of parameters each client uploads is $\mathcal{O}(Bd_r)$, which is much smaller than the number of model parameters (detailed numerical results in Table 1). The computation cost at client in training FL round can be summarized as $\mathcal{O}(I(3FE + 2FF + 2FD))$, where FE , FF , and FD represent the computation cost of encoder en , W_n , and decoder de respectively for a batch in the forward propagation. Given the light weight of W_n , most of additional computation cost results from encoding the augmented data. In Appendix C.3, we further provide detailed comparison of computation and communication complexity among FUELS and state-of-the-art methods.

5. Experiments

In this section, we conduct extensive experiments to validate the effectiveness and efficiency of our proposed FUELS to answer the following research questions: **RQ1**: Can FUELS achieve dominant prediction performance with the baselines in a communication-efficient manner? **RQ2**: Do the periodicity-aware prototypes outperform the concatenation-based prototypes? **RQ3**: How do different loss items in FUELS affect the prediction performance? **RQ4**: Does the dynamic hard negative filtering really work? **RQ5**: How do hyperparameters affect prediction performance?

5.1. Experimental Settings

We evaluate our proposed method on the following three benchmark datasets, i.e., short message services (SMS), voice calls (Call), and Internet services (Net) (Barlacchi et al., 2015). The performance of FUELS is compared with 6 popular FL methods, including FedAvg (McMahan et al., 2017), FedProx (Li et al., 2020), FedRep (Collins et al., 2021), PerFedAvg (Fallah et al., 2020), pFedMe (Dinh et al., 2020), FedDA (Zhang et al., 2021), and Solo. We adopt two widely used metrics to evaluate the prediction performance, i.e., Mean Squared Error (MSE) and Mean Absolute Error (MAE). Due to space limitation, detailed introduction of experimental settings is presented in Appendix D.1.

5.2. Performance Comparison (RQ1)

The evaluation results of the baselines and our proposed method on three datasets are presented in Table 1. We have

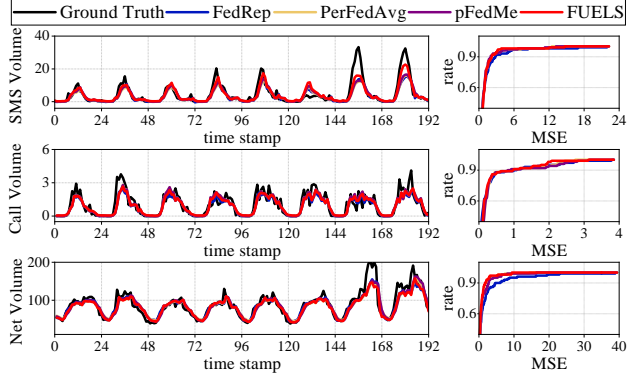


Figure 3. Comparison of different methods in terms of prediction values and CDFs of MSE.

the key observations that FUELS shows promising performance by consistently outperforming all the baselines on the three datasets. Moreover, the communication cost of clients in FUELS is significantly lower than that in the baselines, with approximate 94% reduction in communication parameters per client at each round. We attribute the superiority to the designed contrastive tasks and novel communication carrier.

Effectiveness. Figure 3 shows the predicted values of four methods and the cumulative distribution functions (CDFs) of MSEs over all clients. We observe that the predicted values of FedRep, PerFedAvg, pFedMe and FUELS have similar prediction performance at the smooth traffic sequences. However, FUELS can generate more accurate results in fluctuating traffic sequences on all three datasets. The area under the CDF curve of FUELS is larger than those of the other three methods, which indicates that clients’ prediction MSEs in FUELS distribute around lower values. Taking the Net dataset for example, 87% of clients have prediction MSEs lower than 1.5, while the cases for FedRep, pFedMe and PerFedAvg are 72%, 80% and 81% respectively.

Efficiency. Figure 4 further shows the training MSE versus the communication amounts over all clients. We observe that given the same MSE, the communication amounts in pFedMe and FedRep are significantly higher than those in FUELS on both datasets. FUELS can yield superior prediction performance with the baselines and simultaneously reduce the communication cost to a great extent, which indicates the efficiency of FUELS.

5.3. Ablation Study (RQ2, RQ3 and RQ4)

we compare FUELS with the following 4 variants. (1) **w/o inter (for RQ3)**: Only the intra-client contrastive loss item is adopted; (2) **w/o intra (for RQ3)**: Only the inter-client contrastive loss item is adopted; (3) **w/o p-aware**

Table 1. Performance comparison of different methods on three benchmark datasets. “# of Comm Params” refers to the averaged number of parameters each client sends to the server per round. “Average” represents the averaging performance on three datasets.

Dataset Metric	SMS		Call		Net		Average		# of Comm Params
	MSE	MAE	MSE	MAE	MSE	MAE	MSE	MAE	
Solo	1.884	0.604	0.361	0.294	2.423	0.654	1.556	0.517	-
FedAvg	1.452	0.533	0.393	0.300	2.649	0.638	1.498	0.490	100737
FedProx	1.495	0.542	0.394	0.300	2.528	0.629	1.472	0.490	100737
FedRep	1.551	0.557	0.372	0.299	2.288	0.625	1.404	0.494	100737
PerFedAvg	1.253	0.553	0.392	0.336	1.107	0.543	0.917	0.478	100737
pFedMe	1.250	0.549	0.409	0.335	1.184	0.546	0.948	0.476	100737
FedDA	1.937	0.699	1.055	0.430	3.589	0.849	2.193	0.659	100737
FUELS	1.249	0.541	0.353	0.311	0.880	0.488	0.827	0.446	6144

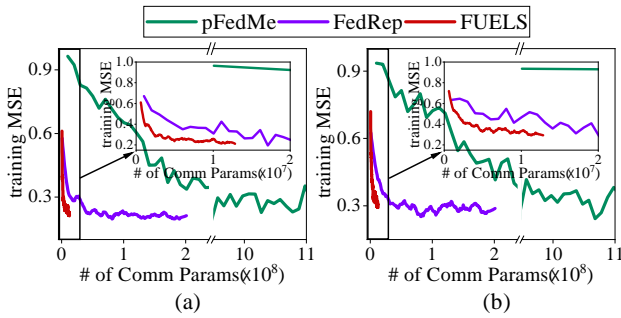


Figure 4. Training MSE versus communication amounts on (a) SMS and (b) Net datasets.

(for RQ2): Concatenation-based prototypes are adopted instead of periodicity-aware prototypes; (4) w/o W (for RQ4): Dynamic hard negative filtering is omitted. The prediction performance of FUELS and the above variants on Net dataset is shown in Figure 5. Full results are presented in Table 7.

We have the following key observations. (1) The increased prediction errors of w/o inter and w/o intra compared with FUELS indicate that inter- and intra-client contrastive loss items can benefit the local training from different perspectives. (2) With concatenation-based prototypes, the prediction performance may be impacted by the noise in representations and “# of Comm Params” will significantly increase to 227328. (3) The higher error in w/o W indicates that the proposed dynamic filtering module can effectively filter out hard negatives and keep the semantic structure consistent.

5.4. Hyperparameter Investigation (RQ5)

We investigate the effects of different settings of β , τ , and ρ on prediction performance, which is shown in Figure 6. (1) β affects how the server divides the positive and negative sets for clients. Too larger or lower values of β will make

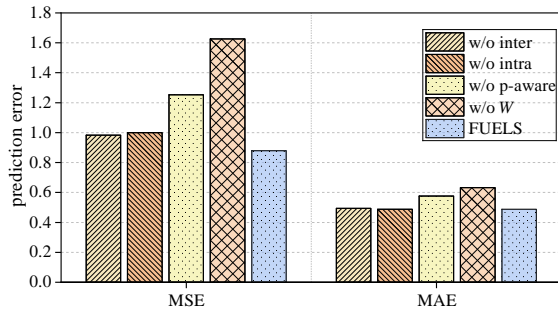


Figure 5. Performance comparison of FUELS and four variants on Net dataset.

the server fail to strike the balance between guaranteeing the spatial heterogeneity and sharing similar knowledge. When β is set as the 50-th percentile of all JSD values, FUELS achieves the best performance. (2) A lower value of τ will make the contrastive loss pay more attention to punishing the negative samples (Wang & Liu, 2021). In general, MSE gets higher with the increase of τ and we finally set τ as 0.02. (3) Different settings of ρ determine how deep clients pay attention to the spatial heterogeneity. To keep a balance between the temporal and spatial heterogeneity, ρ should be neither too high nor too low. From Figure 6(c), the best setting of ρ is 5.

5.5. Case Study

Relatedness Between Local Prototype and Traffic Data.

We randomly select several clients to visualize the correlation between prototypes and local datasets. The results are shown in Figure 8(a) and (b). We calculate the similarity of local training datasets based on JSD and set the threshold as 0.00065, which is also the 50-th percentile of these JSD values. We observe that clients’ correlation illustrated in Figure 8(a) is the same as the JSD-based results in Figure 8(b). Therefore, we claim that the designed local prototypes can effectively express client-specific knowledge.

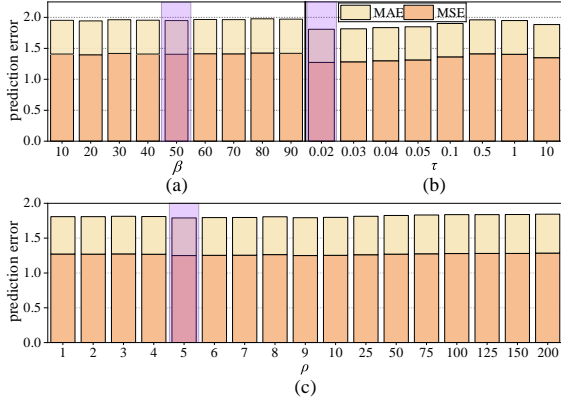


Figure 6. Different settings of (a) β , (b) τ , and (c) ρ versus prediction errors on SMS dataset.

Visualization of Dynamic Hard Negative Filtering. The illustration of parameters in W_n for a randomly selected client is presented in Figure 9. If a parameter in W_n is over 0, the corresponding value in Z will be over 0, otherwise equal to 0. Almost all the values on the diagonal are less than 0, which represents that positives are filtered out. Furthermore, the filtering approach can filter out hard negatives within or without closeness scope and simultaneously avoid the error filtering of true negatives within closeness range.

5.6. Combination with Privacy Mechanisms

We incorporate FUELS with privacy-preserving mechanisms in case of the privacy leakage in the communicated prototypes. Similar to differential privacy, **we add different types of random noise with Laplace, Guassian, and exponential distribution to the local prototypes in FUELS.** The results indicate that there is no significant performance degradation in the performance of FUELS after noise injection. Details are presented in D.2.

5.7. Additional Experimental Results in Appendix

Due to space limitation, we provide auxiliary experimental results in Appendix, including **effect of prototype size** (in Appendix D.3) and **performance on extra dataset** (Appendix D.4).

6. Related Work

6.1. Federated Learning for Spatio-Temporal Forecasting

Due to the effectiveness of FL, there have been many works focusing on incorporating FL into spatio-temporal forecasting tasks, e.g., wireless traffic prediction (Zhang et al., 2021; Perifanis et al., 2023; Zhang et al., 2022). These FL methods focus on how to evaluate the decoupled spatial and

temporal correlation at the server and at the clients respectively by split learning (Meng et al., 2021), clustering (Liu et al., 2020; Zhang et al., 2021), online learning (Liu et al., 2023), and so on. However, all of these methods ignore the spatio-temporal heterogeneity and yield prediction results for different time stamps or different clients with the shared parameter space.

6.2. Personalized Federated Learning

Personalized federated learning (PFL) tackles with the problem of inference performance decline aroused by statistics heterogeneity across clients. The existing PFL methods can be divided into 2 categories, i.e., clients training a global model or training personalized local models. Methods in the first category aim to increase the generalization of the global model by designing client-selection strategy (Yang et al., 2021; Li et al., 2021a) or adding proximal item to original functions (Karimireddy et al., 2020; Li et al., 2021b) In the second category, researchers modify the conventional FL procedure by network splitting (Arivazhagan et al., 2019; Bui et al., 2019; Liang et al., 2020), multitask learning (Smith et al., 2017; Ghosh et al., 2020; Xie et al., 2021), knowledge distillation (Li & Wang, 2019; Zhu et al., 2021b; Lin et al., 2020) and so on. However, all of these works fail to solve the decoupled spatio-temporal heterogeneity.

6.3. Contrastive Learning

In contrastive learning, embeddings from similar samples are pulled closer and those from different ones are pushed away by constraining the loss function (Chen et al., 2020; He et al., 2020). Due to its effectiveness, contrastive learning has been applied to many scenarios, i.e., graph learning (Li et al., 2022; You et al., 2020; Zhu et al., 2021a), traffic flow prediction (Ji et al., 2023; Yue et al., 2022; Woo et al., 2022), etc. Furthermore, some researches have focused on introducing contrastive learning into PFL paradigm mainly for handling statistics heterogeneity (Li et al., 2021b; Tan et al., 2022b; Yu et al., 2022; Mu et al., 2023). However, all of these methods focus on improving the performance on image classification. How to tackle with the spatio-temporal heterogeneity PFL paradigm by contrastive learning remains an open problem.

7. Conclusion and Future Work

We propose FUELS for tackling the spatio-temporal heterogeneity. Specifically, we adaptively align the temporal and spatial representations according to semantic similarity for the supplemented intra- and inter-client contrastive tasks to preserve the spatio-temporal heterogeneity in the latent representation space. Note-worthily, a lightweight but efficient prototype is designed as the client-level representation for carrying client-specific knowledge. Experimental results

demonstrate the effectiveness and efficiency of FUELS.

Due to the ubiquity of spatio-temporal heterogeneity, FUELS may be also applicable to other spatio-temporal tasks. Since the communication carrier is independent of network structures, FUELS can be built over heterogeneous local prediction models, pre-trained models, or even Large Language Models, which will be explored in future studies.

Impact Statements

This paper presents work whose goal is to advance the field of Machine Learning. There are many potential societal consequences of our work, none which we feel must be specifically highlighted here.

References

- Arivazhagan, M. G., Aggarwal, V., Singh, A. K., and Choudhary, S. Federated learning with personalization layers. *arXiv preprint arXiv:1912.00818*, 2019.
- Barlacchi, G., De Nadai, M., Larcher, R., Casella, A., Chitic, C., Torrisi, G., Antonelli, F., Vespignani, A., Pentland, A., and Lepri, B. A multi-source dataset of urban life in the city of milan and the province of trentino. *Scientific data*, 2(1):1–15, 2015.
- Bui, D., Malik, K., Goetz, J., Liu, H., Moon, S., Kumar, A., and Shin, K. G. Federated user representation learning. *arXiv preprint arXiv:1909.12535*, 2019.
- Chen, D., Yao, L., Gao, D., Ding, B., and Li, Y. Efficient personalized federated learning via sparse model-adaptation. *arXiv preprint arXiv:2305.02776*, 2023.
- Chen, T., Kornblith, S., Norouzi, M., and Hinton, G. A simple framework for contrastive learning of visual representations. In *International conference on machine learning*, pp. 1597–1607. PMLR, 2020.
- Collins, L., Hassani, H., Mokhtari, A., and Shakkottai, S. Exploiting shared representations for personalized federated learning. In *International conference on machine learning*, pp. 2089–2099. PMLR, 2021.
- Dinh, C. T., Tran, N. H., and Nguyen, T. D. Personalized federated learning with moreau envelopes. In *Advances in Neural Information Processing Systems 2020, NeurIPS 2020, December 6-12, 2020*.
- Fallah, A., Mokhtari, A., and Ozdaglar, A. Personalized federated learning with theoretical guarantees: A model-agnostic meta-learning approach. *Advances in Neural Information Processing Systems*, 33:3557–3568, 2020.
- Ghosh, A., Chung, J., Yin, D., and Ramchandran, K. An efficient framework for clustered federated learning. *Advances in Neural Information Processing Systems*, 33: 19586–19597, 2020.
- He, K., Fan, H., Wu, Y., Xie, S., and Girshick, R. Momentum contrast for unsupervised visual representation learning. In *Proceedings of the IEEE/CVF conference on computer vision and pattern recognition*, pp. 9729–9738, 2020.
- Ji, J., Wang, J., Huang, C., Wu, J., Xu, B., Wu, Z., Zhang, J., and Zheng, Y. Spatio-temporal self-supervised learning for traffic flow prediction. In *Proceedings of the AAAI Conference on Artificial Intelligence*, volume 37, pp. 4356–4364, 2023.
- Kairouz, P., McMahan, H. B., Avent, B., Bellet, A., Bennis, M., Bhagoji, A. N., Bonawitz, K., Charles, Z., Cormode, G., Cummings, R., et al. Advances and open problems in federated learning. *Foundations and Trends® in Machine Learning*, 14(1–2):1–210, 2021.
- Karimireddy, S. P., Kale, S., Mohri, M., Reddi, S., Stich, S., and Suresh, A. T. Scaffold: Stochastic controlled averaging for federated learning. In *International conference on machine learning*, pp. 5132–5143. PMLR, 2020.
- Kingma, D. P. and Ba, J. Adam: A method for stochastic optimization. *arXiv preprint arXiv:1412.6980*, 2014.
- Langley, P. Crafting papers on machine learning. In Langley, P. (ed.), *Proceedings of the 17th International Conference on Machine Learning (ICML 2000)*, pp. 1207–1216, Stanford, CA, 2000. Morgan Kaufmann.
- Li, D. and Wang, J. Fedmd: Heterogenous federated learning via model distillation. *arXiv preprint arXiv:1910.03581*, 2019.
- Li, L., Duan, M., Liu, D., Zhang, Y., Ren, A., Chen, X., Tan, Y., and Wang, C. Fedsae: A novel self-adaptive federated learning framework in heterogeneous systems. In *2021 International Joint Conference on Neural Networks (IJCNN)*, pp. 1–10. IEEE, 2021a.
- Li, M. and Zhu, Z. Spatial-temporal fusion graph neural networks for traffic flow forecasting. In *Proceedings of the AAAI conference on artificial intelligence*, volume 35, pp. 4189–4196, 2021.
- Li, Q., He, B., and Song, D. Model-contrastive federated learning. In *Proceedings of the IEEE/CVF conference on computer vision and pattern recognition*, pp. 10713–10722, 2021b.
- Li, R., Zhong, T., Jiang, X., Trajcevski, G., Wu, J., and Zhou, F. Mining spatio-temporal relations via self-paced

- graph contrastive learning. In *Proceedings of the 28th ACM SIGKDD Conference on Knowledge Discovery and Data Mining*, pp. 936–944, 2022.
- Li, T., Sahu, A. K., Zaheer, M., Sanjabi, M., Talwalkar, A., and Smith, V. Federated optimization in heterogeneous networks. *Proceedings of Machine learning and systems*, 2:429–450, 2020.
- Li, W. and Wang, S. Federated meta-learning for spatial-temporal prediction. *Neural Computing and Applications*, 34(13):10355–10374, 2022.
- Li, Y., Yu, R., Shahabi, C., and Liu, Y. Diffusion convolutional recurrent neural network: Data-driven traffic forecasting. In *International Conference on Learning Representations (ICLR '18)*, 2018.
- Li, Y., Li, J., and Wang, Y. Privacy-preserving spatiotemporal scenario generation of renewable energies: A federated deep generative learning approach. *IEEE Transactions on Industrial Informatics*, 18(4):2310–2320, 2021c.
- Liang, P. P., Liu, T., Ziyin, L., Allen, N. B., Auerbach, R. P., Brent, D., Salakhutdinov, R., and Morency, L.-P. Think locally, act globally: Federated learning with local and global representations. *arXiv preprint arXiv:2001.01523*, 2020.
- Lin, J., Chen, Y., Zheng, H., Ding, M., Cheng, P., and Hanzo, L. A data-driven base station sleeping strategy based on traffic prediction. *IEEE Transactions on Network Science and Engineering*, 2021.
- Lin, T., Kong, L., Stich, S. U., and Jaggi, M. Ensemble distillation for robust model fusion in federated learning. *Advances in Neural Information Processing Systems*, 33: 2351–2363, 2020.
- Liu, Q., Sun, S., Liu, M., Wang, Y., and Gao, B. Online spatio-temporal correlation-based federated learning for traffic flow forecasting. *arXiv preprint arXiv:2302.08658*, 2023.
- Liu, X., Liang, Y., Huang, C., Zheng, Y., Hooi, B., and Zimmermann, R. When do contrastive learning signals help spatio-temporal graph forecasting? In *Proceedings of the 30th International Conference on Advances in Geographic Information Systems*, pp. 1–12, 2022.
- Liu, Y., James, J., Kang, J., Niyato, D., and Zhang, S. Privacy-preserving traffic flow prediction: A federated learning approach. *IEEE Internet of Things Journal*, 7(8): 7751–7763, 2020.
- Mahdy, B., Abbas, H., Hassanein, H. S., Noureldin, A., and Abou-zeid, H. A clustering-driven approach to predict the traffic load of mobile networks for the analysis of base stations deployment. *Journal of Sensor and Actuator Networks*, 9(4):53, 2020.
- McMahan, B., Moore, E., Ramage, D., Hampson, S., and y Arcas, B. A. Communication-efficient learning of deep networks from decentralized data. In *Artificial intelligence and statistics*, pp. 1273–1282. PMLR, 2017.
- Meng, C., Rambhatla, S., and Liu, Y. Cross-node federated graph neural network for spatio-temporal data modeling. In *Proceedings of the 27th ACM SIGKDD conference on knowledge discovery & data mining*, pp. 1202–1211, 2021.
- Mu, X., Shen, Y., Cheng, K., Geng, X., Fu, J., Zhang, T., and Zhang, Z. Fedproc: Prototypical contrastive federated learning on non-iid data. *Future Generation Computer Systems*, 143:93–104, 2023.
- Perifanis, V., Pavlidis, N., Koutsiamanis, R.-A., and Efraimidis, P. S. Federated learning for 5g base station traffic forecasting. *Computer Networks*, 235:109950, 2023.
- Smith, V., Chiang, C.-K., Sanjabi, M., and Talwalkar, A. S. Federated multi-task learning. *Advances in neural information processing systems*, 30, 2017.
- Tan, A. Z., Yu, H., Cui, L., and Yang, Q. Towards personalized federated learning. *IEEE Transactions on Neural Networks and Learning Systems*, 2022a.
- Tan, Y., Long, G., Ma, J., Liu, L., Zhou, T., and Jiang, J. Federated learning from pre-trained models: A contrastive learning approach. *Advances in Neural Information Processing Systems*, 35:19332–19344, 2022b.
- Wang, F. and Liu, H. Understanding the behaviour of contrastive loss. In *Proceedings of the IEEE/CVF conference on computer vision and pattern recognition*, pp. 2495–2504, 2021.
- Woo, G., Liu, C., Sahoo, D., Kumar, A., and Hoi, S. Cost: Contrastive learning of disentangled seasonal-trend representations for time series forecasting. *arXiv preprint arXiv:2202.01575*, 2022.
- Xie, M., Long, G., Shen, T., Zhou, T., Wang, X., Jiang, J., and Zhang, C. Multi-center federated learning. *arXiv preprint arXiv:2108.08647*, 2021.
- Yang, M., Wang, X., Zhu, H., Wang, H., and Qian, H. Federated learning with class imbalance reduction. In *2021 29th European Signal Processing Conference (EU-SIPCO)*, pp. 2174–2178. IEEE, 2021.
- You, Y., Chen, T., Sui, Y., Chen, T., Wang, Z., and Shen, Y. Graph contrastive learning with augmentations. *Advances*

in neural information processing systems, 33:5812–5823, 2020.

Yu, Q., Liu, Y., Wang, Y., Xu, K., and Liu, J. Multimodal federated learning via contrastive representation ensemble. In *The Eleventh International Conference on Learning Representations*, 2022.

Yue, Z., Wang, Y., Duan, J., Yang, T., Huang, C., Tong, Y., and Xu, B. Ts2vec: Towards universal representation of time series. In *Proceedings of the AAAI Conference on Artificial Intelligence*, volume 36, pp. 8980–8987, 2022.

Zhang, C., Dang, S., Shihada, B., and Alouini, M.-S. Dual attention-based federated learning for wireless traffic prediction. In *IEEE INFOCOM 2021-IEEE conference on computer communications*, pp. 1–10. IEEE, 2021.

Zhang, L., Zhang, C., and Shihada, B. Efficient wireless traffic prediction at the edge: A federated meta-learning approach. *IEEE Communications Letters*, 26(7):1573–1577, 2022.

Zhao, S., Jiang, X., Jacobson, G., Jana, R., Hsu, W.-L., Rustamov, R., Talasila, M., Aftab, S. A., Chen, Y., and Borcea, C. Cellular network traffic prediction incorporating handover: A graph convolutional approach. In *2020 17th Annual IEEE International Conference on Sensing, Communication, and Networking (SECON)*, pp. 1–9. IEEE, 2020.

Zhu, Y. and Wang, S. Joint traffic prediction and base station sleeping for energy saving in cellular networks. In *ICC 2021-IEEE International Conference on Communications*, pp. 1–6. IEEE, 2021.

Zhu, Y., Xu, Y., Yu, F., Liu, Q., Wu, S., and Wang, L. Graph contrastive learning with adaptive augmentation. In *Proceedings of the Web Conference 2021*, pp. 2069–2080, 2021a.

Zhu, Z., Hong, J., and Zhou, J. Data-free knowledge distillation for heterogeneous federated learning. In *International conference on machine learning*, pp. 12878–12889. PMLR, 2021b.

A. Notations

Table 2. Main notations and descriptions in Section 2 and 3.

Notation	Description
n	Client index
N	Total number of clients
\mathcal{D}_n	Training dataset of client n
$D = \sum_{n=1}^N \mathcal{D}_n $	Total number of training samples of N clients
$(\mathbf{x}_n, \mathbf{y}_n)$	A batch of training samples of client n
$\delta_n = (\delta_n^c, \delta_n^p)$	Encoder’s parameters of client n
ϕ_n	Decoder’s parameters of client n
W_n	Filtering matrix of client n
$w_n = (\delta_n, \phi_n, W_n)$	Local parameters of client n
B	Local batch size
r_n	Representation of \mathbf{x}_n
d_r	Dimension of representation
R_n	Local prototype of client n
$\mathcal{PC}_n, \mathcal{NC}_n$	Positive and negative prototype set of client n
PR_n, NR_n	Global positive and negative prototype of client n
β	JSD threshold
α	Selection ratio
τ	Temperature factor
ρ	Additive weight of \mathcal{L}_{inter}
$\mathcal{L}(\cdot)$	Loss function
$\mathcal{L}_{pred}, \mathcal{L}_{intra}, \mathcal{L}_{inter}$	Loss items for prediction, intra-client contrastive task, and inter-client contrastive task

B. Detailed Procedure of FUELS

The training process of FUELS is presented in Algorithm 1. We elaborate the procedure as follows.

- **Initialization:** At the initial round, all the client participating in FUELS should provide their local prototypes. Similarly, for the clients who want to join during the training stage, they should also provide local prototypes firstly.
- **Aggregation:** After the server receiving local prototypes from participating clients, it will update \mathcal{R} , perform JSD-based aggregation to generate client-customized global prototypes for the next round.
- **Local Training:** Each selected client calculates the representations of the raw and augmented data, computes three loss items gradually and then optimizes the local prediction model. After all batches, it yields the local prototype and uploads to the server.

C. Analysis

C.1. Proof of Generalization Bound

Assumption C.1. (Bounded Maximum) The Loss function $\mathcal{L}(\cdot)$ has an upper bound, i.e., $\max \mathcal{L}(\cdot) \leq C, C < \infty$.

Theorem C.2. (Generalization Bounded) Let $w_n^*, n \in [1, N]$ denote the optimal model parameters for client n by Algorithm 1. Denote the prediction model f as a hypothesis from \mathcal{F} and d as the VC-dimension of \mathcal{F} . With the probability at least $1-\kappa$:

$$\begin{aligned} & \max_{(w_1, \dots, w_N)} \left[\sum_{n=1}^N \frac{|\mathcal{D}_n|}{D} \mathcal{L}(w_n) - \sum_{n=1}^N \frac{|\mathcal{D}_n|}{D} \mathcal{L}(w_n^*) \right] \\ & \leq \sqrt{\frac{2d}{D} \log \frac{eD}{d}} + \sqrt{\frac{C^2 D^2}{2} \log \frac{1}{\kappa}}, \end{aligned}$$

Algorithm 1 Training process of FUELS

Input: $\mathcal{D}_n, \mathcal{D}'_n, n = 1, \dots, N, \rho, \beta, \tau, \alpha$.

1 **SERVEREXECUTE:**

2 Initialize $\{PR_n\}_{n=1}^N$ and $\{NR_n\}_{n=1}^N$.

3 Initialize the set of local prototypes $\mathcal{R} = \emptyset$.

4 **for** $t = 1, 2, \dots, T$ **do**

5 **if** $t = 1$ **then**

6 **for each client** n **in parallel do**

7 $R_n \leftarrow \text{ClientExecute}(n, PR_n, NR_n)$

8 $\mathcal{R} \leftarrow \mathcal{R} + \{R_n\}$

9 **else**

10 Randomly select $N\alpha$ clients.

11 **for each selected client** n **in parallel do**

12 $R_n \leftarrow \text{ClientExecute}(n, PR_n, NR_n)$

13 Update R_n in \mathcal{R} .

14 Yield \mathcal{PC}_n and $\mathcal{RC}_n, n \in [N]$ based on JSD values.

15 $PR_n = \frac{1}{|\mathcal{PC}_n|} \sum_{R_m \in \mathcal{PC}_n} R_m, NR_n = \frac{1}{|\mathcal{NC}_n|} \sum_{R_m \in \mathcal{NC}_n} R_m \forall n \in [N]$.

16 **Function** $\text{ClientExecute}(n, PR_n, NR_n)$:

17 **for each epoch do**

18 Initialize the set of representations $\mathcal{R}_n = \emptyset$.

19 **for** $(\mathbf{x}_n, \mathbf{y}_n)$ in $\mathcal{D}_n, (\mathbf{x}'_n, \mathbf{y}'_n)$ in \mathcal{D}'_n **do**

20 $r_n \leftarrow \text{en}(\delta_n; \mathbf{x}_n), r'_n \leftarrow \text{en}(\delta_n; \mathbf{x}'_n)$

21 $\mathcal{R}_n \leftarrow \mathcal{R}_n + \{r_n\}$

22 Calculate $\mathcal{L}_{intra}, \mathcal{L}_{inter}$, and \mathcal{L}_{pred} via Eq. (6), (11), and (14).

23 $\mathcal{L} \leftarrow \mathcal{L}_{intra} + \mathcal{L}_{inter} + \rho \mathcal{L}_{pred}$

24 Update δ_n and ϕ_n via gradient descent.

25 $R_n \leftarrow \text{AVG}(\mathcal{R}_n)$.

26 **return** R_n

Proof. We denote $g(w_1, \dots, w_N) = \max_{(w_1, \dots, w_N)} \left[\sum_{n=1}^N \frac{|\mathcal{D}_n|}{D} \mathcal{L}(w_n) - \sum_{n=1}^N \frac{|\mathcal{D}_n|}{D} \mathcal{L}(w_n^*) \right]$ and can obtain that

$$\begin{aligned}
 & |g(w_1, \dots, w_n, \dots, w_N) - g(w_1, \dots, w'_n, \dots, w_N)| \\
 &= \left| \max_{(w_1, \dots, w_N)} \left[\sum_{n=1}^N \frac{|\mathcal{D}_n|}{D} \mathcal{L}(w_n) - \sum_{n=1}^N \frac{|\mathcal{D}_n|}{D} \mathcal{L}(w_n^*) \right] - \max_{(w_1, \dots, w'_n, \dots, w_N)} \left[\sum_{n=1}^N \frac{|\mathcal{D}_n|}{D} \mathcal{L}(w'_n) - \sum_{n=1}^N \frac{|\mathcal{D}_n|}{D} \mathcal{L}(w_n^*) \right] \right| \\
 &= \left| \max_{w_n} \left[\frac{|\mathcal{D}_n|}{D} (\mathcal{L}(w_n) - \mathcal{L}(w_n^*)) \right] - \max_{w'_n} \left[\frac{|\mathcal{D}_n|}{D} (\mathcal{L}(w'_n) - \mathcal{L}(w_n^*)) \right] \right| \\
 &= \frac{|\mathcal{D}_n|}{D} \left| \max_{w_n} [\mathcal{L}(w_n) - \mathcal{L}(w_n^*)] - \max_{w'_n} [\mathcal{L}(w'_n) - \mathcal{L}(w_n^*)] \right| \\
 &= \frac{|\mathcal{D}_n|}{D} \left| \max_{w_n, w'_n} [\mathcal{L}(w_n) - \mathcal{L}(w'_n) + \mathcal{L}(w'_n) - \mathcal{L}(w_n^*)] - \max_{w'_n} [\mathcal{L}(w'_n) - \mathcal{L}(w_n^*)] \right| \\
 &\leq \frac{|\mathcal{D}_n|}{D} \left| \max_{w_n, w'_n} [\mathcal{L}(w_n) - \mathcal{L}(w'_n)] \right| \\
 &\stackrel{(a)}{\leq} \frac{C|\mathcal{D}_n|^2}{D}
 \end{aligned} \tag{20}$$

(a) follows Assumption C.1. Therefore, g is difference bounded. From the McDiarmid's inequality, we have

$$\mathbb{P}[g(w_1, \dots, w_N) - \mathbb{E}[g(w_1, \dots, w_N)] \geq \varepsilon] \leq \exp\left(-\frac{2\varepsilon^2}{\sum_{n=1}^N c_n^2}\right), \quad (21)$$

where $c_n = \frac{C|\mathcal{D}_n|^2}{D}$. (21) can be transformed into

$$\mathbb{P}[g(w_1, \dots, w_N) - \mathbb{E}[g(w_1, \dots, w_N)] \leq \varepsilon] \geq 1 - \exp\left(-\frac{2\varepsilon^2}{\sum_{n=1}^N c_n^2}\right), \quad (22)$$

which indicates that with probability at least $1 - \exp\left(-\frac{2\varepsilon^2}{\sum_{n=1}^N c_n^2}\right)$,

$$g(w_1, \dots, w_N) - \mathbb{E}[g(w_1, \dots, w_N)] \leq \varepsilon \quad (23)$$

Let $\kappa = \exp\left(-\frac{2\varepsilon^2}{\sum_{n=1}^N c_n^2}\right)$, and

$$\begin{aligned} \varepsilon &= \sqrt{\frac{\sum_{n=1}^N c_n^2}{2} \ln \frac{1}{\kappa}} \\ &= \sqrt{\frac{\sum_{n=1}^N \left(\frac{C|\mathcal{D}_n|^2}{D}\right)^2}{2} \log \frac{1}{\kappa}} \\ &\leq \sqrt{\frac{\frac{C^2}{D^2} \left(\sum_{n=1}^N |\mathcal{D}_n|^2\right)^2}{2} \log \frac{1}{\kappa}} \\ &\leq \sqrt{\frac{\frac{C^2}{D^2} \left(\sum_{n=1}^N |\mathcal{D}_n|\right)^4}{2} \log \frac{1}{\kappa}} \\ &= \sqrt{\frac{C^2 D^2}{2} \log \frac{1}{\kappa}} \end{aligned} \quad (24)$$

Therefore, (23) can be transformed into

$$\begin{aligned} &\max_{(w_1, \dots, w_N)} \left[\sum_{n=1}^N \frac{|\mathcal{D}_n|}{D} \mathcal{L}(w_n) - \sum_{n=1}^N \frac{|\mathcal{D}_n|}{D} \mathcal{L}(w_n^*) \right] \\ &\leq \mathbb{E} \left\{ \max_{(w_1, \dots, w_N)} \left[\sum_{n=1}^N \frac{|\mathcal{D}_n|}{D} \mathcal{L}(w_n) - \sum_{n=1}^N \frac{|\mathcal{D}_n|}{D} \mathcal{L}(w_n^*) \right] \right\} + \sqrt{\frac{C^2 D^2}{2} \log \frac{1}{\kappa}}. \end{aligned} \quad (25)$$

We then calculate the upper bound of the first term in the right hand.

$$\begin{aligned}
 & \mathbb{E} \left\{ \max_{(w_1, \dots, w_N)} \left[\sum_{n=1}^N \frac{|\mathcal{D}_n|}{D} \mathcal{L}(w_n) - \sum_{n=1}^N \frac{|\mathcal{D}_n|}{D} \mathcal{L}(w_n^*) \right] \right\} \\
 & \leq \mathbb{E} \left\{ \sum_{n=1}^N \frac{|\mathcal{D}_n|}{D} \max_{w_n} [\mathcal{L}(w_n) - \mathcal{L}(w_n^*)] \right\} \\
 & \leq \sum_{n=1}^N \frac{|\mathcal{D}_n|}{D} \mathbb{E} \left\{ \sup_{f \in \mathcal{F}} [\mathcal{L}(w_n) - \mathcal{L}(w_n^*)] \right\} \\
 & \stackrel{(b)}{=} \sum_{n=1}^N \frac{|\mathcal{D}_n|}{D} \mathfrak{R}_n(\mathcal{F}) \\
 & \leq \sum_{n=1}^N \frac{|\mathcal{D}_n|}{D} \sqrt{\frac{2d}{|\mathcal{D}_n|} \log \frac{e|\mathcal{D}_n|}{d}} \\
 & \stackrel{(c)}{\leq} \sqrt{\frac{2d}{D} \log \frac{eD}{d}}, \tag{26}
 \end{aligned}$$

where \mathcal{F} is the hypothesis set of the prediction model f and d is the VC-dimension of \mathcal{F} . (b) follows the definition of Rademacher complexity and Sauer's Lemma and (c) follows Jensen's inequality.

Therefore,

$$\begin{aligned}
 & \max_{(w_1, \dots, w_N)} \left[\sum_{n=1}^N \frac{|\mathcal{D}_n|}{D} \mathcal{L}(w_n) - \sum_{n=1}^N \frac{|\mathcal{D}_n|}{D} \mathcal{L}(w_n^*) \right] \\
 & \leq \sqrt{\frac{2d}{D} \log \frac{eD}{d}} + \sqrt{\frac{C^2 D^2}{2} \log \frac{1}{\kappa}}. \tag{27}
 \end{aligned}$$

□

C.2. Proof of Convergence Rate

Let $w_{n,t}^i$ denote the local model parameters of client n at the i -th iteration in the t -th FL round, where $0 \leq t \leq T - 1$ and $0 \leq i \leq I - 1$. T and I denote the total number of FL rounds and local iterations respectively. $w_{n,t}^I$ represents the local model parameters of client n after I iterations in the t -th FL round. We denote $w_{n,t+1} = w_{n,t}^I$, which represents the local model of client n in the $t + 1$ round before the first iteration.

Assumption C.3. (*Bounded Expectation of Gradients*) The expectation of gradient of loss function $\mathcal{L}(\cdot)$ is uniformly bounded, i.e., $\mathbb{E}(\|\nabla \mathcal{L}(\cdot)\|) \leq G$.

Assumption C.4. (*Lipschitz Smooth*) The loss function \mathcal{L} is L_1 -smooth, i.e., $\mathcal{L}(w) - \mathcal{L}(w') \leq \langle \nabla \mathcal{L}(w'), w - w' \rangle + L_1 \|w - w'\|^2, \forall w, w', \exists L_1 > 0$.

Assumption C.5. (*Lipschitz Continuity*) Suppose $h : \mathcal{A}_1 \times \mathcal{A}_2 \times \dots \rightarrow \mathcal{A}_T$ is Lipschitz Continuous in \mathcal{A}_j , i.e., $\exists L_h, \forall a_j, \hat{a}_j \in \mathcal{A}_j, \|h(a_1, \dots, a_j, \dots) - h(a_1, \dots, \hat{a}_j, \dots)\| \leq L_h \|a_j - \hat{a}_j\|$.

Theorem C.6. (*Convergence Rate*) Let Assumption C.3 to C.5 hold. Let $\mathcal{L}(w_{n,0}^0) - \mathcal{L}(w_n^*) = \Lambda$. If clients adopt stochastic gradient descent method to optimize local prediction models with the learning rate equal to η , for any client, given $\xi > 0$, after

$$T = \frac{\Lambda}{\xi I (\eta - L_1 \eta^2) - \rho \eta L_h N \alpha I^2 G}$$

FL rounds, we can obtain

$$\frac{1}{TI} \sum_{t=0}^{T-1} \sum_{i=0}^{I-1} \mathbb{E} \left[\|\nabla \mathcal{L}(w_{n,t}^i)\|^2 \right] < \xi$$

with

$$\eta < \frac{\xi - \rho L_h N \alpha I G}{L_1 \xi}.$$

Proof. Let Assumption C.4 hold, we have

$$\mathcal{L}(w_{n,t}^1) \leq \mathcal{L}(w_{n,t}^0) + \langle \nabla \mathcal{L}(w_{n,t}^0), (w_{n,t}^1 - w_{n,t}^0) \rangle + L_1 \|w_{n,t}^1 - w_{n,t}^0\|^2. \quad (28)$$

With $w_{n,t}^1 = w_{n,t}^0 - \eta \nabla \mathcal{L}(w_{n,t}^0)$, it can be transformed into

$$\begin{aligned} \mathcal{L}(w_{n,t}^1) &\leq \mathcal{L}(w_{n,t}^0) - \eta \langle \nabla \mathcal{L}(w_{n,t}^0), \nabla \mathcal{L}(w_{n,t}^0) \rangle + L_1 \eta^2 \|\nabla \mathcal{L}(w_{n,t}^0)\|^2 \\ &= \mathcal{L}(w_{n,t}^0) - \eta \|\nabla \mathcal{L}(w_{n,t}^0)\|^2 + L_1 \eta^2 \|\nabla \mathcal{L}(w_{n,t}^0)\|^2. \end{aligned} \quad (29)$$

We can obtain

$$\begin{aligned} \mathcal{L}(w_{n,t}^1) &\leq \mathcal{L}(w_{n,t}^0) - (\eta - L_1 \eta^2) \|\nabla \mathcal{L}(w_{n,t}^0)\|^2 \\ \mathcal{L}(w_{n,t}^2) &\leq \mathcal{L}(w_{n,t}^1) - (\eta - L_1 \eta^2) \|\nabla \mathcal{L}(w_{n,t}^1)\|^2 \\ &\vdots \\ \mathcal{L}(w_{n,t+1}) &= \mathcal{L}(w_{n,t}^I) \leq \mathcal{L}(w_{n,t}^{I-1}) - (\eta - L_1 \eta^2) \|\nabla \mathcal{L}(w_{n,t}^{I-1})\|^2. \end{aligned}$$

Therefore,

$$\mathcal{L}(w_{n,t+1}) \leq \mathcal{L}(w_{n,t}^0) - (\eta - L_1 \eta^2) \sum_{i=1}^I \|\nabla \mathcal{L}(w_{n,t}^{i-1})\|^2. \quad (30)$$

Furthermore, we have

$$\mathcal{L}(w_{n,t+1}^0) = \mathcal{L}(w_{n,t+1}) + \mathcal{L}(w_{n,t+1}^0) - \mathcal{L}(w_{n,t+1}). \quad (31)$$

With (16),

$$\begin{aligned} &\mathcal{L}(w_{n,t+1}^0) - \mathcal{L}(w_{n,t+1}) \\ &= \mathcal{L}_{pred}(\delta_{n,t+1}, \phi_{n,t+1}) + \mathcal{L}_{intra}(\delta_{n,t+1}, W_{n,t+1}) + \rho \mathcal{L}_{inter}(\delta_{n,t+1}; PR_{n,t+1}, NR_{n,t+1}) \\ &\quad - \mathcal{L}_{pred}(\delta_{n,t}, \phi_{n,t}) - \mathcal{L}_{intra}(\delta_{n,t}, W_{n,t}) - \rho \mathcal{L}_{inter}(\delta_{n,t}; PR_{n,t}, NR_{n,t}) \\ &= \rho \{ \mathcal{L}_{inter}(\delta_{n,t+1}; PR_{n,t+1}, NR_{n,t+1}) - \mathcal{L}_{inter}(\delta_{n,t}; PR_{n,t}, NR_{n,t}) \}. \end{aligned} \quad (32)$$

Thereinto, $\delta_{n,t}$ denotes the encoder parameters of client n at the t -th round. $PR_{n,t}$ and $NR_{n,t}$ represent the global positive and negative prototype for client n respectively at the t -th round. We have

$$\begin{aligned} PR_{n,t} &= \frac{1}{|\mathcal{PC}_{n,t}|} \sum_{m \in \mathcal{PC}_{n,t}} R_{m,t} \\ &= \frac{1}{|\mathcal{PC}_{n,t}|} \sum_{m \in \mathcal{PC}_{n,t}} \left[\frac{1}{I} \sum_{i=0}^{I-1} en(\delta_{m,t-1}^i) \right] \\ &= \frac{1}{I |\mathcal{PC}_{n,t}|} \sum_{m \in \mathcal{PC}_{n,t}} \sum_{i=0}^{I-1} en(\delta_{m,t-1}^i), \end{aligned} \quad (33)$$

where $\mathcal{PC}_{n,t}$ denotes the positive set of client n in the t -th round. Similarly,

$$NR_{n,t} = \frac{1}{I |\mathcal{NC}_{n,t}|} \sum_{m \in \mathcal{NC}_{n,t}} \sum_{i=0}^{I-1} en(\delta_{m,t-1}^i). \quad (34)$$

Therefore,

$$\begin{aligned} &\mathcal{L}_{inter}(\delta_{n,t+1}; PR_{n,t}, NR_{n,t}) \\ &= \mathcal{L}_{inter} \left(\delta_{n,t+1}; \frac{1}{I |\mathcal{PC}_{n,t}|} \sum_{m \in \mathcal{PC}_{n,t}} \sum_{i=0}^{I-1} en(\delta_{m,t-1}^i), \frac{1}{I |\mathcal{NC}_{n,t}|} \sum_{m \in \mathcal{NC}_{n,t}} \sum_{i=0}^{I-1} en(\delta_{m,t-1}^i) \right) \\ &\triangleq h \left(\delta_{1,t-1}^0, \delta_{1,t-1}^1, \dots, \delta_{1,t-1}^{I-1}, \dots, \delta_{N,t-1}^0, \delta_{N,t-1}^1, \dots, \delta_{N,t-1}^{I-1} \right). \end{aligned} \quad (35)$$

We can treat \mathcal{L}_{inter} as a multivariate function h with NI variants, i.e., $\delta_{m,t-1}^i$, $1 \leq m \leq N$, and $0 \leq i \leq I-1$. We make the assumption that h is Lipschitz continuous. Following Assumption C.5, we have $\exists L_h > 0$,

$$\begin{aligned} & \left\| h \left(\delta_{1,t-1}^0, \delta_{1,t-1}^1, \dots, \delta_{1,t-1}^{I-1}, \dots, \delta_{N,t-1}^0, \delta_{N,t-1}^1, \dots, \delta_{N,t-1}^{I-1} \right) \right. \\ & \quad \left. - h \left(\hat{\delta}_{1,t-1}^0, \hat{\delta}_{1,t-1}^1, \dots, \hat{\delta}_{1,t-1}^{I-1}, \dots, \hat{\delta}_{N,t-1}^0, \hat{\delta}_{N,t-1}^1, \dots, \hat{\delta}_{N,t-1}^{I-1} \right) \right\| \\ & \leq L_h \left\| \delta_{1,t-1}^0 - \hat{\delta}_{1,t-1}^0 \right\|. \end{aligned} \quad (36)$$

Therefore,

$$\begin{aligned} & \mathcal{L}_{inter}(\delta_{n,t+1}; PR_{t+1}, NR_{t+1}) - \mathcal{L}_{inter}(\delta_{n,t+1}; PR_{n,t}, NR_{n,t}) \\ & = h \left(\delta_{1,t}^0, \delta_{1,t}^1, \dots, \delta_{1,t}^{I-1}, \dots, \delta_{N,t}^0, \delta_{N,t}^1, \dots, \delta_{N,t}^{I-1} \right) - h \left(\delta_{1,t-1}^0, \delta_{1,t-1}^1, \dots, \delta_{1,t-1}^{I-1}, \dots, \delta_{N,t-1}^0, \delta_{N,t-1}^1, \dots, \delta_{N,t-1}^{I-1} \right) \\ & \leq \left\| h \left(\delta_{1,t}^0, \delta_{1,t}^1, \dots, \delta_{1,t}^{I-1}, \dots, \delta_{N,t}^0, \delta_{N,t}^1, \dots, \delta_{N,t}^{I-1} \right) - h \left(\delta_{1,t-1}^0, \delta_{1,t-1}^1, \dots, \delta_{1,t-1}^{I-1}, \dots, \delta_{N,t-1}^0, \delta_{N,t-1}^1, \dots, \delta_{N,t-1}^{I-1} \right) \right\| \\ & \leq L_h \left(\sum_{m \in \mathcal{SC}_t} \sum_{i=0}^{I-1} \left\| \delta_{m,t}^i - \delta_{m,t-1}^i \right\| \right), \end{aligned} \quad (37)$$

where \mathcal{SC}_t represents the set of selected $N\alpha$ clients in the t -th FL round.

Therefore, (31) can be transformed into

$$\begin{aligned} \mathcal{L}(w_{n,t+1}^0) & = \mathcal{L}(w_{n,t+1}) + \mathcal{L}(w_{n,t+1}^0) - \mathcal{L}(w_{n,t+1}) \\ & \leq \mathcal{L}(w_{n,t+1}) + \rho L_h \left(\sum_{m \in \mathcal{SC}_t} \sum_{i=0}^{I-1} \left\| \delta_{m,t}^i - \delta_{m,t-1}^i \right\| \right) \\ & = \mathcal{L}(w_{n,t+1}) + \rho L_h \sum_{m \in \mathcal{SC}_t} \sum_{i=0}^{I-1} \left\| \sum_{j=i}^{I-1} \eta \Delta w_{m,t-1}^j + \sum_{j=0}^{i-1} \eta \Delta w_{m,t}^j \right\|. \end{aligned} \quad (38)$$

Take expectations on both sides, we have

$$\begin{aligned} \mathbb{E}[\mathcal{L}(w_{n,t+1}^0)] & \leq \mathcal{L}(w_{n,t+1}) + \rho L_h \sum_{m \in \mathcal{SC}_t} \sum_{i=0}^{I-1} \left\| \sum_{j=i}^{I-1} \eta \mathbb{E}[\Delta w_{m,t-1}^j] + \sum_{j=0}^{i-1} \eta \mathbb{E}[\Delta w_{m,t}^j] \right\| \\ & \leq \mathcal{L}(w_{n,t+1}) + \rho L_h \sum_{m \in \mathcal{SC}_t} \sum_{i=0}^{I-1} \eta IG \\ & \leq \mathcal{L}(w_{n,t+1}) + \rho \eta L_h N \alpha I^2 G \end{aligned} \quad (39)$$

By incorporating (30) with (39), we can obtain

$$\mathbb{E}[\mathcal{L}(w_{n,t+1}^0)] \leq \mathcal{L}(w_{n,t}^0) + \rho \eta L_h N \alpha I^2 G - (\eta - L_1 \eta^2) \sum_{i=0}^{I-1} \left\| \nabla \mathcal{L}(w_{n,t}^i) \right\|^2. \quad (40)$$

To ensure

$$\rho \eta L_h N \alpha I^2 G - (\eta - L_1 \eta^2) \sum_{i=0}^{I-1} \left\| \nabla \mathcal{L}(w_{n,t}^i) \right\|^2 \leq 0, \quad (41)$$

we can obtain

$$\eta \leq \frac{\sum_{i=0}^{I-1} \left\| \nabla \mathcal{L}(w_{n,t}^i) \right\|^2 - \rho L_h N \alpha I^2 G}{L_1 \sum_{i=0}^{I-1} \left\| \nabla \mathcal{L}(w_{n,t}^i) \right\|^2}. \quad (42)$$

Considering all the FL rounds, i.e., $0 \leq t \leq T - 1$, with (40), we have

$$\sum_{t=0}^{T-1} \mathbb{E} [\mathcal{L}(w_{n,t+1}^0)] \leq \sum_{t=0}^{T-1} \mathcal{L}(w_{n,t}^0) + T\rho\eta L_h N\alpha I^2 G - (\eta - L_1\eta^2) \sum_{t=0}^{T-1} \sum_{i=0}^{I-1} \mathbb{E} [\|\nabla \mathcal{L}(w_{n,t}^i)\|^2], \quad (43)$$

which can be transformed into

$$\frac{1}{TI} \sum_{t=0}^{T-1} \sum_{i=0}^{I-1} \mathbb{E} [\|\nabla \mathcal{L}(w_{n,t}^i)\|^2] \leq \frac{\frac{1}{TI} \sum_{t=0}^{T-1} \{\mathcal{L}(w_{n,t}^0) - E[\mathcal{L}(w_{n,t+1}^0)]\} + \rho\eta L_h N\alpha IG}{\eta - L_1\eta^2}. \quad (44)$$

Suppose $\mathcal{L}(w_{n,0}^0) - \mathcal{L}(w_n^*) = \Lambda$,

$$\frac{\frac{1}{TI} \sum_{t=0}^{T-1} \{\mathcal{L}(w_{n,t}^0) - E[\mathcal{L}(w_{n,t+1}^0)]\} + \rho\eta L_h N\alpha IG}{\eta - L_1\eta^2} < \frac{\frac{\Lambda}{TI} + \rho\eta L_h N\alpha IG}{\eta - L_1\eta^2} < \xi. \quad (45)$$

Therefore, we can obtain that, with

$$T > \frac{\Lambda}{\xi I(\eta - L_1\eta^2) - \rho\eta L_h N\alpha I^2 G}, \quad (46)$$

$$\frac{1}{TI} \sum_{t=0}^{T-1} \sum_{i=0}^{I-1} \mathbb{E} [\|\nabla \mathcal{L}(w_{n,t}^i)\|^2] < \xi, \quad (47)$$

if

$$\eta \leq \frac{\sum_{i=0}^{I-1} \|\nabla \mathcal{L}(w_{n,t}^i)\|^2 - \rho L_h N\alpha I^2 G}{L_1 \sum_{i=0}^{I-1} \|\nabla \mathcal{L}(w_{n,t}^i)\|^2} < \frac{I\xi - \rho L_h N\alpha I^2 G}{L_1 I\xi} = \frac{\xi - \rho L_h N\alpha IG}{L_1 \xi}. \quad (48)$$

□

Table 3. Comparison of FUELS and three baselines in terms of communication parameters (*Comm*) and computation cost (*Comp*). $|w|$ and $|\delta|$ denote the number of parameters in prediction model and in the encoder respectively. I' denotes the number of batches of the test dataset. \mathcal{T} in PerFedAvg denotes the number of local gradient descent steps.

	<i>Comm</i>		<i>Comp</i>		
	Client	Server	Train (Client)	Infer (Client)	Train (Server)
FedAvg	$\mathcal{O}(w)$	$\mathcal{O}(N\alpha w)$	$\mathcal{O}(2I(FE + FD))$	$\mathcal{O}(I'(FE + FD))$	$\mathcal{O}(1)$
FedRep	$\mathcal{O}(\delta)$	$\mathcal{O}(N\alpha \delta)$	$\mathcal{O}(2I(FE + FD))$	$\mathcal{O}(I'(FE + FD))$	$\mathcal{O}(1)$
PerFedAvg	$\mathcal{O}(w)$	$\mathcal{O}(N\alpha w)$	$\mathcal{O}(6\mathcal{T}(FE + FD))$	$\mathcal{O}((I' + 2)(FE + FD))$	$\mathcal{O}(1)$
FUELS	$\mathcal{O}(Bd_r)$	$\mathcal{O}(2N\alpha Bd_r)$	$\mathcal{O}(I(3FE + 2FF + 2FD))$	$\mathcal{O}(I'(FE + FD))$	$\mathcal{O}\left(\left(\alpha - \frac{\alpha^2}{2}\right)N^2 - \frac{\alpha}{2}N\right)$

C.3. Complexity Analysis

We compare the computation cost and the number of communication parameters in FUELS with three personalized FL methods, which is presented in Table 3. *Comm* represents the number of parameters each client (the server) transmitted to the server (all the selected clients) each round. The 4-th and 6-th rows in Table 3 present the computation cost of a client and the server in each FL training round respectively. *Comp* in the inference stage represents the computation cost for inferring the total test dataset.

Compared with the other methods based on model transmission, FUELS is highly communication-efficient, i.e., $Bd_r \ll |\delta| < |w|$. In the forward propagation, FUELS should encode the augmented data for the subsequent intra-client contrastive task, and hence resulting in more computation cost in the training stage. The server should update the JSD matrix according to the fresh local prototypes to generate the customized global prototypes for the next round. We deem that the introduced computation cost at the server can be overlooked, given the abundant resources of the server.

D. Experimental Details and Additional Results

D.1. Experimental Details

Datasets. The adopted dataset is from the Big Data Challenge programmed by the Telecom Italia (Barlacchi et al., 2015). The area of Trentino is divided into 6575 cells with size of 235×235 meters, which is shown in Figure 7. The dataset includes three types of Call Detail Records (CDRs), i.e., Short Message Services (SMS), Voice Calls (Call), and Internet Services (Net), detected from 2013/11/01 to 2014/01/01 every 10 minutes. The diversity of traffic data from different cells exhibits the spatial heterogeneity. For example, the traffic data of the cells in different function zones may have diverse temporal patterns, i.e., traffic distribution in downtown area is quite different from that in suburb area.

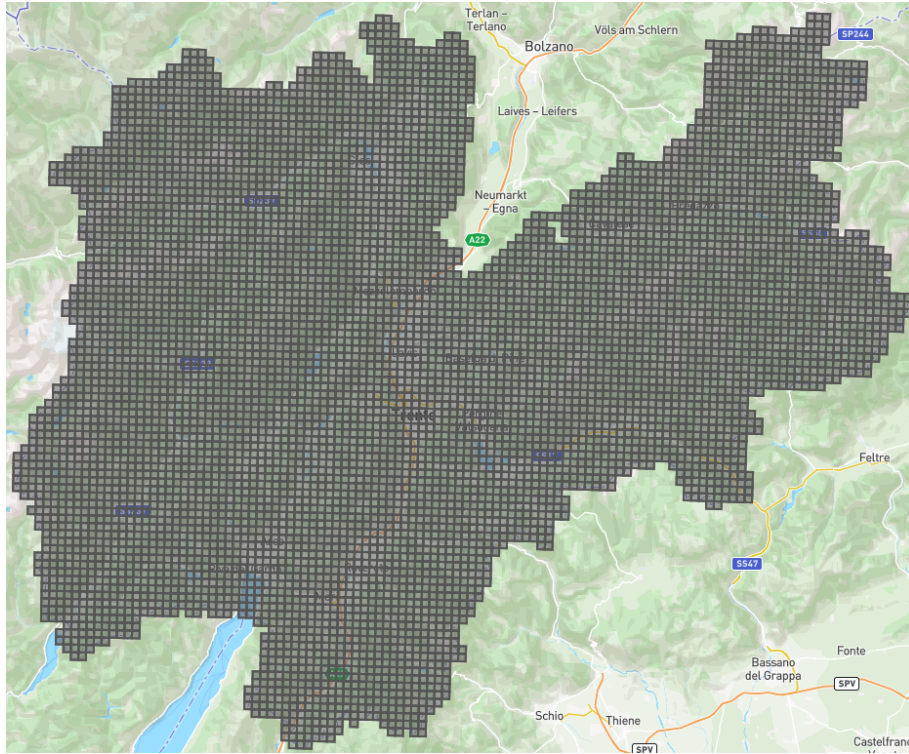


Figure 7. The division of Trentino.

Baselines. We compare the performance of FUELS with the following baselines.

- **Solo:** All clients train their own local prediction models using local data and do not communicate with each other or with the server.
- **FedAvg** (McMahan et al., 2017): It is a classical FL method, where the server aggregates the local model updates via averaging strategy.
- **FedProx** (Li et al., 2020): Compared with FedAvg, a proximal term is added to the local loss function for tackling with the statistical heterogeneity.
- **FedRep** (Collins et al., 2021): In this method, only parameters of low layers (encoder in our paper) are communicated between clients and the server for learning shared representations. Each client maintains its personalized head (decoder in our paper) for the final prediction.
- **PerFedAvg** (Fallah et al., 2020): This method aims to train an initial model which can quickly adapt to clients' local data via several steps of gradient descent.
- **pFedMe** (Dinh et al., 2020): In this method, by the designed regularized loss function, each client can train the global model and simultaneously optimize the personalized model.

- **FedDA** (Zhang et al., 2021): In this method, the server firstly train a initial global model via the uploaded augmented data from clients. In the FL training stage, the server aggregates local models by the designed dual attention mechanism.

Experimental Setup. To tackle with the problem of data sparsity, traffic data are resampled every 1 hour as per (Zhang et al., 2021). Without loss of generality, we randomly select 100 cells as the clients, i.e., $N = 100$. The experimental setup of FedDA complies with the corresponding literature, unless stated otherwise. The experimental settings of the other baselines are the same as FUELS for the sake of fairness. In our experiments, the GRU_c and GRU_p all have 1 GRU layer with 128 cells. The decoder is a fully-connected layer. The batch size B is set to 24. The closeness window c and periodic window q are both set to 3. The temperature rate τ is set to 0.02. For each dataset, we set β as the 50-th percentile of all JSD values. The training round of FUELS T is set to 200, and each client transmits periodicity-aware prototypes to the server after conducting local training for 1 epoch at each round. We use an Adam optimizer with the learning rate 0.001 (Kingma & Ba, 2014).

D.2. Privacy Protection

The widely adopted differential privacy in FL framework for preserving privacy is based on adding random noise with *Laplace*, *Guassian*, or *exponential* distribution to the uploaded model parameters. However, this approach may perturb the model parameters, thus worsening the final prediction performance. Similarly, we add various random noise to the communicated local prototypes. The performance comparison is presented in Table 4. We observe that FUELS with different types of random noise can always achieve the superior performance, compared with FedAvg. Moreover, FUELS promises the combination of privacy-preserving techniques without significant performance decrease.

Table 4. The performance of FUELS with different types of privacy-preserving mechanisms. μ and λ denote the mean value and the standard deviation of the corresponding noise distribution.

Dataset Metric	SMS		Call		Net	
	MSE	MAE	MSE	MAE	MSE	MAE
FedAvg	1.452	0.533	0.393	0.300	2.649	0.638
FUELS	1.249	0.541	0.353	0.311	0.880	0.488
FUELS + <i>Laplace</i> ($\mu = 0, \lambda = 1$)	1.397	0.563	0.443	0.335	1.086	0.531
FUELS + <i>Guassian</i> ($\mu = 0, \lambda = 1$)	1.395	0.564	0.419	0.328	1.117	0.531
FUELS + <i>exponential</i> ($\lambda = 1$)	1.365	0.554	0.406	0.320	1.047	0.514

D.3. Effect of Prototype Size

The performance of FUELS with different setting of d_r is presented in Table 5. Prototype size can be adjusted for different prediction tasks. In general, better performance can be achieved with d_r increasing, which on the other hand results in more computing and communication overhead.

Table 5. The performance of FUELS with different settings of prototype size.

d_r	SMS		Call		Net		# of Comm Params
	MSE	MAE	MSE	MAE	MSE	MAE	
2	3.588	1.125	1.692	0.848	4.500	1.213	96
4	2.910	0.899	1.265	0.634	3.899	1.041	192
8	2.060	0.683	0.775	0.429	2.559	0.791	384
16	1.709	0.611	0.568	0.364	2.039	0.672	768
32	1.445	0.567	0.471	0.340	1.289	0.562	1536
64	1.348	0.551	0.412	0.321	1.051	0.517	3072
128	1.249	0.541	0.353	0.311	0.880	0.488	6144
256	1.272	0.531	0.318	0.298	0.997	0.487	12288
512	1.248	0.538	0.326	0.300	0.990	0.486	24576

D.4. Results on Other Dataset

We conduct further experiments on the METR-LA, a widely-used dataset in the task of traffic flow forecasting. It includes traffic speed records of 207 loop detectors deployed in Los Angeles from 2012/01/01 to 2012/06/30 every 5 minutes. The experimental settings on METR-LA are the same as those on the other three datasets in Section 5.1. The experimental results of FUELS and baselines are presented in Table 6. It is obvious that FUELS can also achieve the dominate performance compared with the baselines.

Table 6. Numerical results on METR-LA dataset.

Metric	FedAvg	FedProx	FedRep	PerFedAvg	pFedMe	FUELS
MSE	0.126	0.127	0.127	0.143	0.137	0.125
MAE	0.167	0.166	0.164	0.193	0.173	0.166

Table 7. Numerical results of FUELS and four variants on SMS, Call, and Net datasets.

Dataset	SMS		Call		Net	
	MSE	MAE	MSE	MAE	MSE	MAE
w/o inter	1.340	0.560	0.392	0.323	0.983	0.494
w/o intra	1.336	0.566	0.455	0.334	1.000	0.488
w/o p-aware	1.324	0.575	0.400	0.342	1.252	0.570
w/o W	1.480	0.582	0.445	0.337	1.627	0.633
FUELS	1.249	0.541	0.353	0.311	0.880	0.488

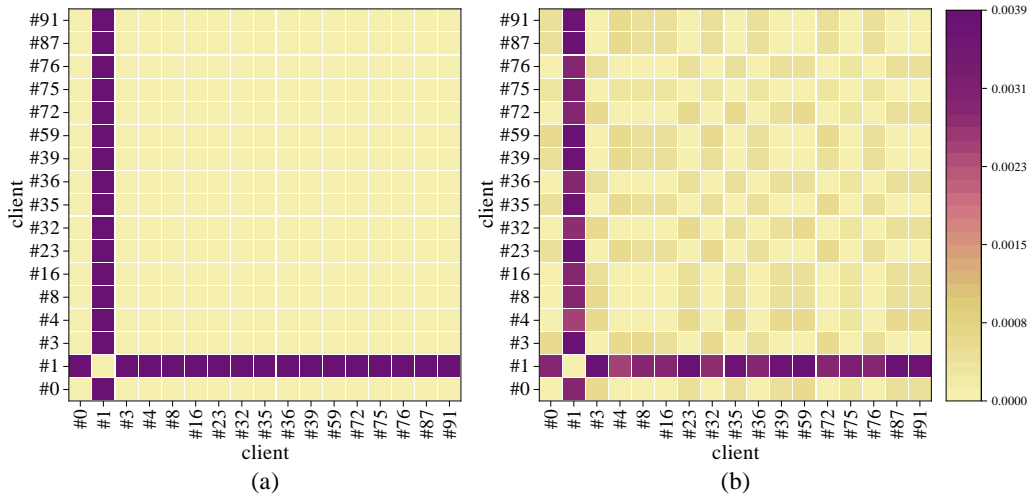


Figure 8. Results of JSD results for (a) local prototypes and (b) raw traffic data. In (a), if the JSD value of two local prototypes is less than β , the corresponding space is marked in yellow, otherwise in purple.

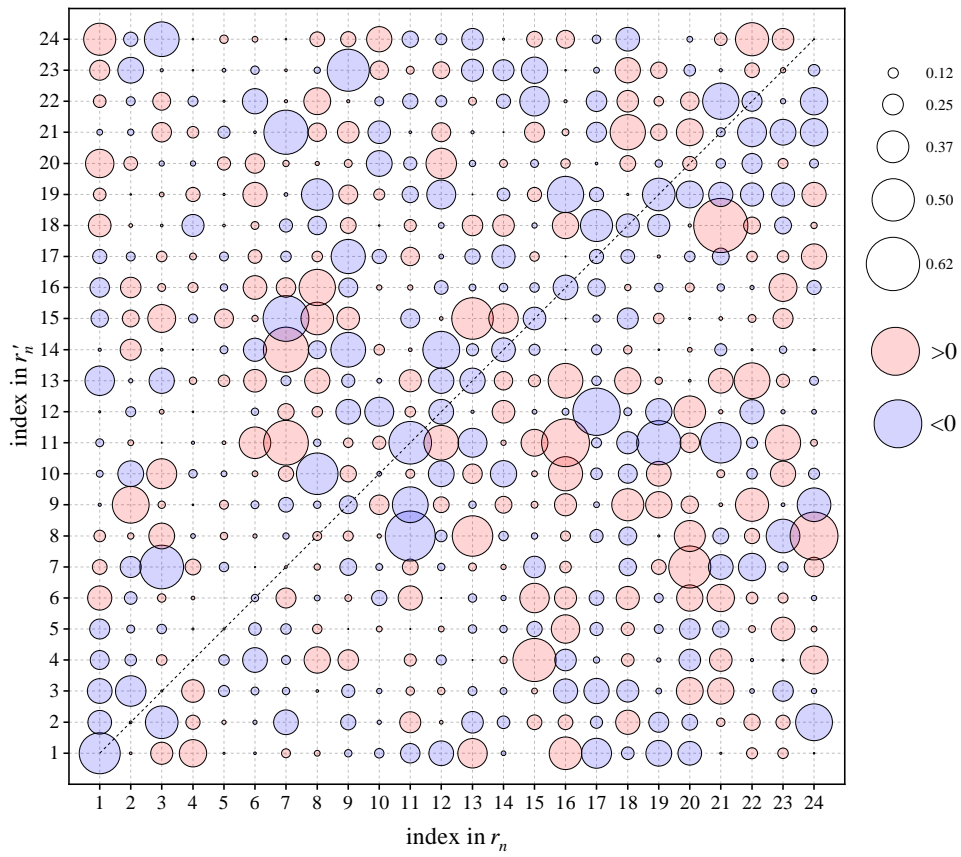


Figure 9. Visualization of W_n . The circle size represents the absolute value of a parameter. If a parameter is over 0, it is marked in pink, otherwise in purple.